Received Date: Sept. 2024 Revised: Nov. 2024 Accepted: Dec. 2024

Bio-based *Acacia catechu*/Ferric Oxide Nanostructured Composite Electrodes for Advanced Energy Storage Materials

Dibyashree Shrestha Ph.D.
Department of Chemistry
Institute of Science and Technology
Patan Multiple Campus, Tribhuvan University, Nepal
Corresponding author : shresthadibyashree@gmail.com (D. Shrestha).
Doi: https://doi.org/10.3126/pragya.v13i2.78781

Abstract

This study explores the bio-based nanocomposite electrodes for advanced energy storage, combining nanostructured ferric oxide (Fe_2O_3) with highly porous activated carbon (PAC) derived from Acacia catechu wood waste. Instrumental analysis confirmed the PAC's desirable structural characteristics, including high surface area and porosity, suitable for electrochemical applications. Initial evaluation of the PAC electrode revealed a specific capacitance of 57.4 Fg^{-1} at 1 Ag^{-1}, 79.1% capacitance retention after 1 000 cycles, and an energy density of 4.8 Wh kg^{-1} at a power density of 159.1 W kg^{-1}. Significantly, compositing PAC with Fe_2O_3 at a 1:1 ratio dramatically enhanced electrochemical performance. The resulting 1:1 (PAC:Fe) nanocomposite exhibited a superior specific capacitance of 104.3 F g^{-1} at 1 Ag^{-1}, a remarkable 96.3% capacitance retention after 1000 cycles, and an elevated energy density of 8.3 Wh kg^{-1} at a power density of 275.0 W kg^{-1}, achieved in a 6 M KOH electrolyte using a three -electrode setup with a 1.55 V working voltage.

Keywords: *Acacia catechu*, ferric oxide, nanocomposite, energy density, electrochemical performance

1. Introduction

The escalating demand for efficient and sustainable energy storage solutions has spurred intensive research into advanced electrode materials. Among these, biomass-derived Activated Carbon (AC) and transition metal oxides like Ferric Oxide (Fe_2O_3) have garnered significant attention (Arun et al., 2019). However, achieving a synergistic combination that maximizes both energy density and cycling stability remains a challenge. In this context, the study introduces a novel approach by utilizing *Acacia catechu* wood waste, an abundantly available and underutilized resource in Nepal, as a precursor for highly porous AC, and integrating it with nanostructured Fe_2O_3 to create a high-performance hybrid electrode.

Acacia catechu (Khair) in the Terai and lower hills of Nepal presents an opportunity for sustainable AC production. Its inherent lignocellulosic composition and local abundance offer a compelling alternative to conventional AC sources, aligning with principles of resource efficiency and environmental stewardship (Kumari, et al., 2022). The novelty of this approach lies in the strategic utilization of *Acacia catechu* wood waste, thereby transforming a readily available waste stream into a valuable resource for advanced energy storage.

While AC is renowned for its high surface area, porosity, and conductivity, offering excellent electric double-layer capacitance (EDLC), its energy density remains limited. Conversely, Fe_2O_3, a cost-effective and abundant transition metal oxide, provides high theoretical pseudo capacitance but suffers from poor conductivity and volume expansion during cycling. Our research addresses these limitations by fabricating a hybrid electrode where nanostructured Fe_2O_3 is intimately combined with *Acacia catechu*-derived AC. This integration aims to leverage the synergistic effects of both materials: the high conductivity and porosity of AC facilitating ion transport, and the pseudocapacitive properties of Fe_2O_3 enhancing energy density.

The precise control of the AC:Fe_2O_3 ratio is crucial for optimizing the electrochemical performance. The study systematically investigates the impact of 1:1 AC to Fe_2O_3 ratio (Gao et al., 2017), (Shrestha, 2022a) on the structural and electrochemical properties of the hybrid electrode. This approach allows researchers to identify the optimal composition that maximizes both specific capacitance and cycling stability (Shrestha et al., 2019; Shrestha and Rajbhandari, 2021; Shrestha, 2022b).

The structural and electrochemical properties of the composite material were thoroughly investigated using a comprehensive suite of techniques, including X-ray diffraction (XRD), Raman spectroscopy, Fourier transform infrared spectroscopy (FTIR), scanning electron microscopy (SEM), Brunauer-Emmett-Teller (BET) analysis, cyclic voltammetry (CV), galvanostatic charge/discharge (GCD), and electrochemical impedance spectroscopy (EIS). By employing this multi-faceted characterization, we aim to provide a detailed understanding of the synergistic interactions between *Acacia catechu*-derived AC and nanostructured Fe_2O_3, and to demonstrate the potential of this bio-based hybrid electrode for advanced energy storage applications.

2. Material and Methods

2.1. Material

Discarded timber from *Acacia catechu* (Khair) sourced from regional carpentry operations within Kathmandu served as a primary raw material. All chemical reagents employed in this investigation were of analytical purity and utilized in their delivered state. The production of activated carbon relied on phosphoric acid (H_3PO_4, 85% concentration) as the activating agent, procured from Fischer Scientific, India. Deionized water, produced via double

distillation, was used for all solution preparations and washing procedures. Conductive carbon black, the polymeric binder polyvinylidene fluoride (PVDF), and the solvent N-methyl-2-pyrrolidone (NMP) were supplied by Sigma-Aldrich, USA. Iron(III) oxide (Fe_2O_3), received from APS Ajax Finechem, Australia, and nickel foam, provided by PRED MATERIALS International, were utilized without any prior treatment (Shrestha et al., 2018; Shrestha, 2021).

2.2. Methods

Preparation of Porous Activated Carbon (PAC) from *Acacia catechu*:

Discarded *Acacia catechu* timber was pulverized into a powder and sieved to 150 µm. The powder was impregnated with 85% phosphoric acid (H_3PO_4) at a 1:1 weight ratio and soaked for 24 hours at room temperature. The mixture was then dried at 110°C for 2 hours. Carbonization was conducted under a nitrogen atmosphere at 400°C for 3 hours, with a nitrogen flow rate of 100 mL/min. The carbonized material was cooled, washed with deionized water until neutral pH, and dried at 110°C (Shrestha, 2022c; Shrestha, 2023). The resulting porous activated carbon was designated PAC.

2.3. Physical Characterization of PAC

The synthesized Porous Activated Carbon (PAC) was characterized using: X-ray diffraction (XRD) for crystalline phase identification; Raman spectroscopy for structural defect analysis; Fourier transform infrared spectroscopy (FTIR) for functional group identification; Brunauer-Emmett-Teller (BET) analysis for surface area and porosity determination; and scanning electron microscopy (SEM) for morphological analysis. Guided by precedent in lignocellulosic carbonization studies, a temperature of 400°C was used to prepare activated carbon from *Acacia catechu*.

2.4. Electrode Fabrication

For the fabrication of PAC electrodes, a mixture of PAC, carbon black, and PVDF at an 8:1:1 weight ratio was ground, combined with N-methyl-2-pyrrolidone (NMP) to form a paste, and applied to a 1 cm^2 nickel foam substrate. Hybrid electrode was fabricated using PAC and Fe_2O_3 at 1:1 weight ratios. Both electrodes (PAC and PAC-Fe) were dried at 70°C overnight, pressed at 10 kPa, and soaked in 6 M KOH electrolyte prior to electrochemical testing. Electrical contact was established using copper wire (Shrestha, 2022b; Shrestha, 2023).

2.5. Electrochemical Evaluation

The electrochemical performance of the fabricated electrodes was evaluated in a 6 M KOH electrolyte using a three-electrode system. This system comprised a working electrode (PAC, hybrid composite, or Fe_2O_3), a platinum counter electrode, and an Ag/AgCl reference electrode. All tests were performed at room temperature using a potentiostat/galvanostat (Shrestha, 2022b).

Cyclic Voltammetry (CV) was conducted within potential windows of -1 to -0.2 V for PAC and -1.15 to -0.4 V for hybrid composite (PAC-Fe), at scan rate 100 mVs^{-1}. Galvanostatic charge-discharge (GCD) measurements were performed over the same potential windows, with current densities of 1 A g^{-1}. GCD data was used to determine cyclic stability, Power and energy density. Electrochemical Impedance Spectroscopy (EIS) was conducted from 100 kHz to 0.1 Hz, with a 10 mV perturbation signal. EIS data was analyzed using appropriate software (Shrestha, 2023).

3. Results and Discussion

Guided by precedent in lignocellulosic carbonization studies (Shrestha et al., 2018; Chakraborty et al., 2020; Shrestha, 2021; Shrestha, 2022b; Shrestha, 2023) a temperature of 400°C was used to prepare activated carbon from *Acacia catechu*. This choice facilitated effective carbon formation and porosity development, crucial for subsequent electrochemical applications. The structural and electrochemical properties of the resulting activated carbon and its composites with ferric oxide were then thoroughly investigated

3.1. Structural and Chemical Analysis of PAC

***XRD*:** The X-ray Diffraction (XRD) pattern of the PAC sample (Figure 1) demonstrates its predominantly amorphous nature, a characteristic highly beneficial for supercapacitor applications. The broad diffraction peaks observed at 23.52° and 43.48° correspond to the (002) and (101) planes of amorphous carbon, respectively. These broad peaks indicate a lack of long-range crystalline order and suggest significant structural disorder within the PAC material. This disordered structure is expected to contribute to a high surface area and facilitate efficient ion transport, both of which are critical for achieving high energy and power densities in supercapacitors. The absence of sharp, well-defined peaks confirms a limited degree of graphitization, which is advantageous for maximizing surface area while maintaining good ion accessibility. The observed XRD pattern suggests that the PAC material possesses a favorable amorphous structure for electrochemical energy storage applications (Molina-Sabio et al., 1995; Wang et al., 2013; Gao et al., 2017).

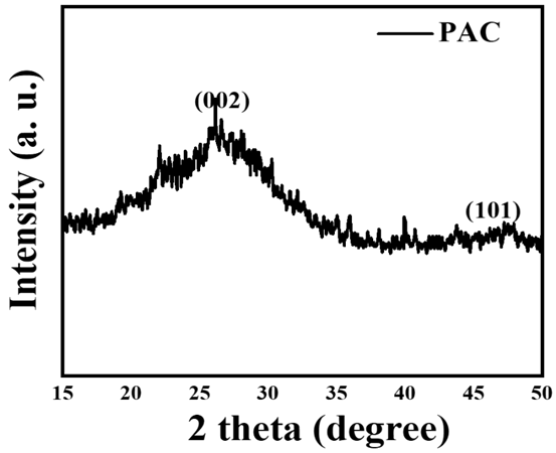

Fig 1: XRD pattern of PAC

Raman Spectra: The Raman spectrum (Fig. 2) of PAC shows two broad peaks: D band (~1344 cm^{-1}) indicating defects and disorder, and the G band (~1587 cm^{-1}) representing graphitic domains. The IG/ID ratio of 1.0 confirms a significant amount of disorder. This disordered structure, consistent with your XRD results, is beneficial for supercapacitors as it provides a high surface area for charge storage and facilitates ion transport. This contributes to the material's high specific capacitance and good rate capability (Gao et al., 2017).

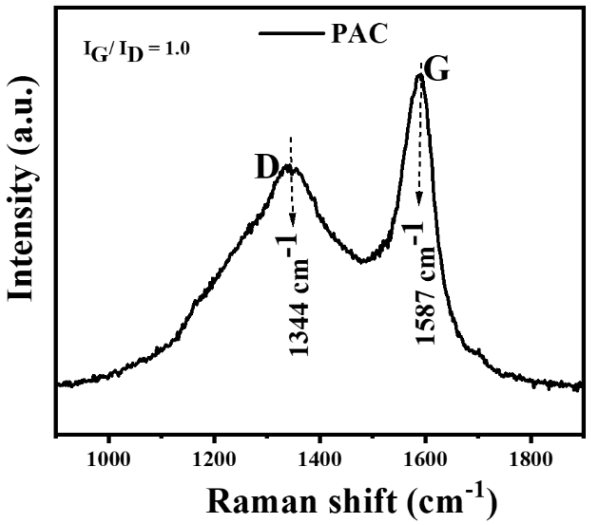

Fig.2: Raman spectra of PAC

SEM: SEM images (Figure 3) at 2000x magnification reveal a highly porous morphology with interconnected pores of varying sizes. This interconnected network attributed to

phosphoric acid activation is expected to provide a high surface area and facilitate ion transport which are crucial for supercapacitor applications (Wang et al., 2013).

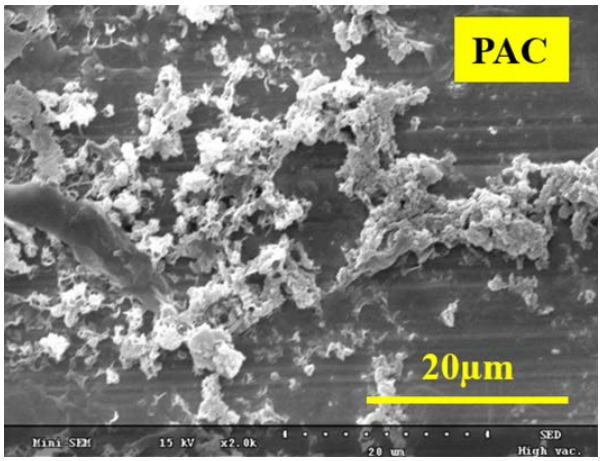

Fig 3: SEM image of PAC

BET Analysis: Figure 4 shows the nitrogen adsorption-desorption isotherm of the PAC sample, which exhibits a **Type IV isotherm with an H4 hysteresis loop**, indicating the presence of mesopores and micropores. The BET surface area was determined to be 989.4 $m^2 g^{-1}$, confirming the high porosity of the material. The pore volume was 1.4 $cm^3 g^{-1}$, and the average pore size was 4.1 nm, suggesting the presence of mesopores. The shape of the hysteresis loop suggests the presence of narrow slit-like pores (Brunauer et al., 1938; Liu et al., 2013).

The high surface area and interconnected pore structure observed in SEM are consistent with the BET results. This porous structure, with a combination of micropores and mesopores, is desirable for supercapacitor applications as it can enhance both charge storage and ion transport. The high surface area is also consistent with the disordered structure observed in XRD and the high defect density indicated by Raman spectroscopy.

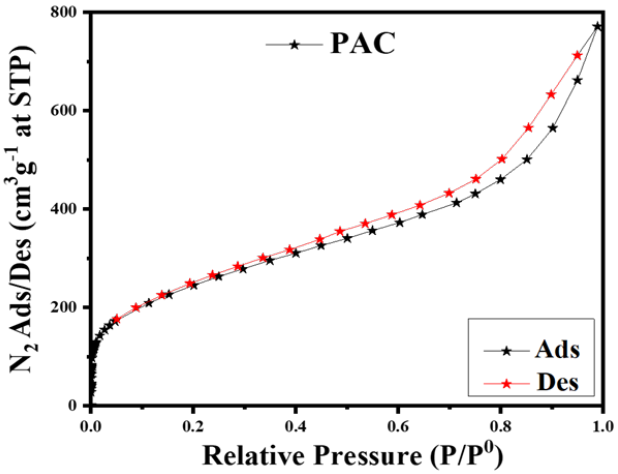

Fig.4: N_2 adsorption/desorption isotherms at 77 K of PAC

FTIR Spectroscopy: Figure 5 shows the FTIR spectrum of the PAC sample. The spectrum reveals several peaks indicative of surface functional groups. A broad peak at 3446 cm^{-1} corresponds to O-H stretching vibrations, suggesting the presence of hydroxyl groups or adsorbed water. The peak at 2936 cm^{-1} is likely due to C-H stretching vibrations of aliphatic groups. The peak at 2361 cm^{-1} is attributed to atmospheric CO_2. A peak at 1590 cm^{-1} could be due to C=C stretching in aromatic rings or C=O stretching in carbonyl groups. The peak at 1084 cm^{-1} is characteristic of C-O stretching vibrations in alcohols, ethers, or carboxylic acids (Sarkar et al., 2015). The presence of these oxygen-containing functional groups is likely a result of the phosphoric acid activation process, which can introduce hydroxyl, carbonyl, and ether groups onto the PAC surface. These functional groups can enhance hydrophilicity and wettability of the PAC, which could be beneficial for supercapacitor applications.

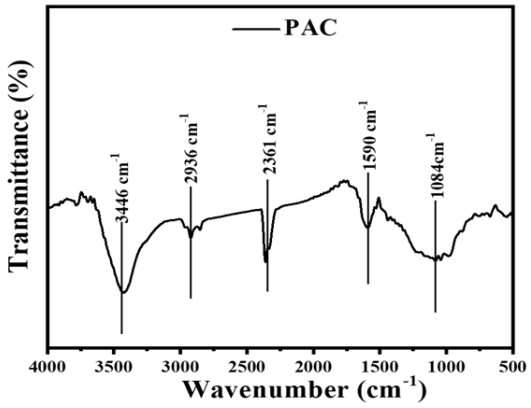

Fig.5: FTIR of PAC

The structural and chemical characterization of the PAC material, as revealed by XRD, Raman spectroscopy, SEM, BET, and FTIR analyses, paints a compelling picture of its potential for energy storage applications. The material exhibits a highly porous architecture with an abundance of oxygen-containing functional groups, both of which are crucial for achieving high electrochemical performance.

With this foundation established, the researchers focus on evaluating the electrochemical behavior of the PAC, both in its pristine form and in composite with ferric oxide. This composite were prepared with a 1:1 ratio of PAC to Fe_2O_3 and are denoted as PAC-Fe. The electrochemical performance of both the pristine PAC and the PAC-Fe composites will be assessed to determine their suitability for energy storage devices.

3.2. Electrochemical performances of electrodes

3.2.1. Cyclic Voltammetry (CV) study

Cyclic voltammetry (CV) was employed to investigate the electrochemical behavior of the PAC electrode and its ferric oxide composite (PAC-Fe) at a scan rate of 100 mVs^{-1}. The potential window for PAC was optimized to -1.0 to -0.2 V, while for PAC-Fe, it was -1.15 to 0.4 V. Figure 6 presents the CV curves obtained for both electrodes.

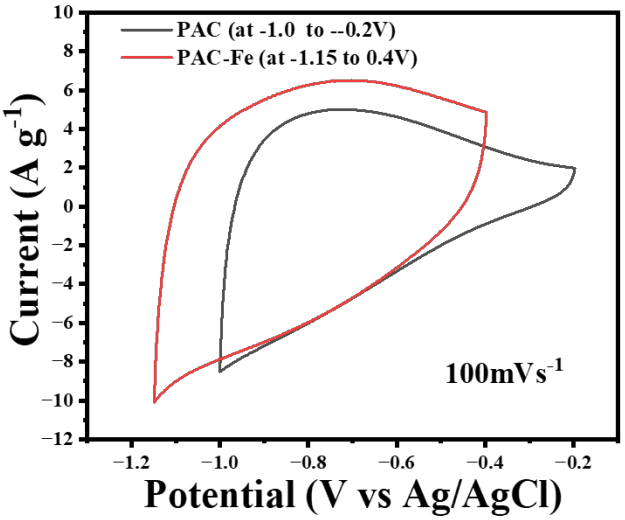

Fig. 6: CV curves of PAC and PAC-Fe electrodes at a scan rate of 100 mVs^{-1}

As presented in Figure 6, the CV curve of PAC exhibits a quasi-rectangular shape, characteristic of electrochemical double-layer capacitance (EDLC) behavior. However, the slight deviation from an ideal rectangle suggests a possible contribution from pseudo capacitance, likely due to surface functional groups present on the PAC material, as evidenced by FTIR analysis (Sinprachim et al., 2016).

In contrast, the CV curve of PAC-Fe displays distinct redox peaks attributed to the reversible Fe^{3+}/Fe^{2+} redox reactions of Fe_2O_3. This indicates a significant contribution from pseudocapacitance in addition to EDLC. The larger integrated area under the PAC-Fe curve compared to the PAC curve suggests a higher charge storage capacity for the composite material (Shrestha and Rajbhandari, 2021; Shrestha, 2022a; Shrestha, 2023).

3.2.2. Galvanostatic Charge/Discharge (GCD) study

Galvanostatic Charge-Discharge (GCD) measurements were performed to further evaluate the electrochemical performance of PAC and PAC-Fe at a current density of 1 A g^{-1} (Figure 7). The potential window for PAC was -1.0 to -0.2 V, and for PAC-Fe it was -1.15 to -0.4 V.

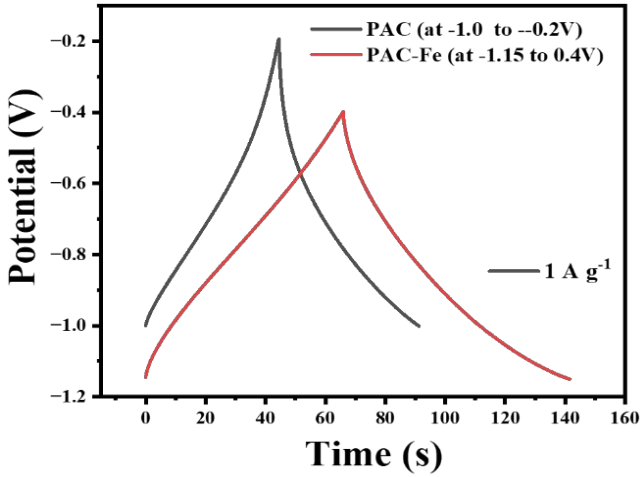

Fig.7: GCD curves of PAC and PAC-Fe electrodes at a current density of 1 Ag^{-1}.

As shown in Figure 7, the GCD curve of PAC exhibits a nearly triangular shape, indicating good charge-discharge reversibility. However, a slight deviation from an ideal triangle suggests some non-ideal capacitive behavior. The discharge time for PAC was approximately 32 seconds.

The GCD curve of PAC-Fe also shows an approximately triangular shape but with distinct bending characteristics, particularly during the discharge process. This bending is attributed to the pseudo capacitance contribution from the Fe^{3+}/Fe^{2+} redox reactions of Fe_2O_3. PAC-Fe displays good symmetry, indicating reversible charge-discharge behavior (Sarangapani, et. al., 1996), (Shrestha, 2023). The discharge time for PAC-Fe was significantly longer, approximately 84 seconds, indicating a higher charge storage capacity compared to PAC.

The specific capacitance (Csp) of the electrodes was calculated using equation (1) (Liu et al., 2013), (Shrestha, 2024).

$$C_{SP} = \frac{I\Delta t}{m\Delta V} \ldots\ldots\ldots\ldots\ldots (1)$$

where I (A) is the discharge current, Δt (s) is the discharge time, ΔV (V) is the potential window, and m (g) is the mass of the active material.

The PAC electrode exhibited a Csp of 57.4 Fg^{-1}. Notably, the PAC-Fe composite demonstrated a significantly higher Csp of 104.3 Fg^{-1} This improved capacitance is attributed to the pseudo capacitance contribution from the Fe_2O_3 component and potentially lower resistance, as will be discussed in the EIS analysis.

3.2.3. Effect of Current Density on Specific Capacitance

The relationship between current density and specific capacitance for PAC and PAC-Fe electrodes is presented in Figure 8. As observed, both electrodes exhibit a decrease in specific capacitance with increasing current density noticeable up to 10 A g^{-1}.

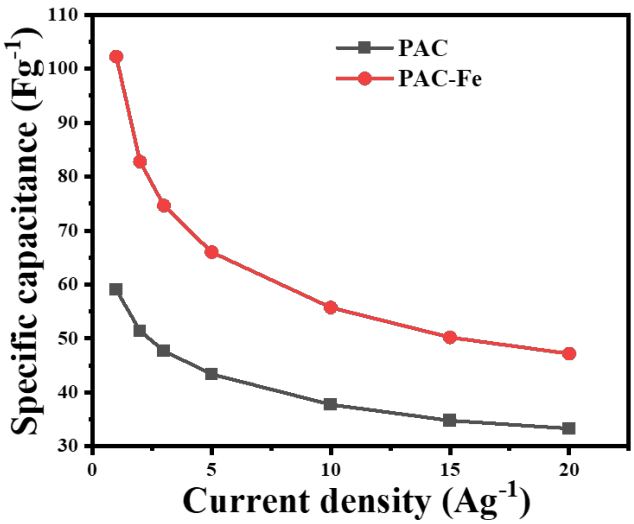

Fig. 8: Specific capacitance of PAC and PAC-Fe electrodes as a function of current density

At a current density of 1 Ag^{-1}, the PAC-Fe composite demonstrates a significantly higher specific capacitance of 104.3 Fg^{-1} compared to the PAC electrode, which exhibits 57.4 Fg^{-1}. This highlights the substantial enhancement in capacitance achieved by incorporating Fe_2O_3 into the PAC matrix. However, the enhancement in capacitance diminishes at higher current densities, as evidenced by the convergence of the two curves.

The reduction in specific capacitance at higher current densities is attributed to the kinetic limitations of ion diffusion. At high current densities, ions struggle to penetrate the inner pores of the electrode material effectively, leading to reduced utilization of the available surface area for charge storage.

3.2.6. Power and energy density evaluation

Ragone plots, derived from galvanostatic charge-discharge measurements, were used to evaluate the power and energy densities of the fabricated electrodes (Figure 9). Energy (E) and power (P) densities were calculated using the following equations:

$$E = \frac{1}{8} C_{SP} \Delta v^2 \quad \text{..... (2)}$$

$$P = \frac{E}{\Delta t} \quad \text{..... (3)}$$

where E is the energy density in Wh kg^{-1}, P is the power density in W kg^{-1}, Csp is the specific capacitance in F g^{-1}, ΔV is the potential window, and Δt (s) is the discharge time. In this study, a three-electrode system was used, hence the energy density was calculated by dividing the specific capacitance by 8 instead of 2 (Shrestha, 2024).

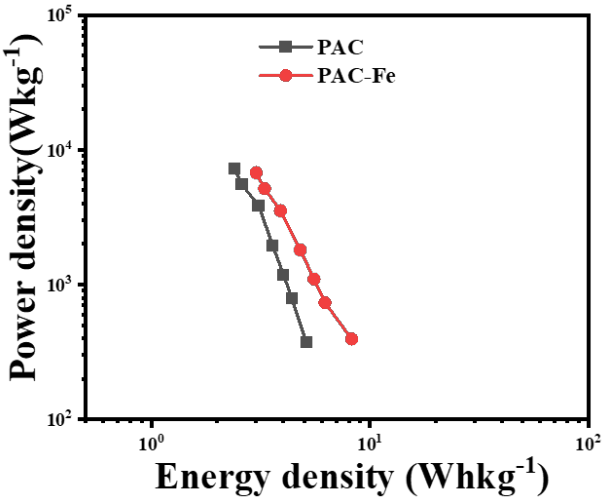

Fig. 9: Ragone plots of PAC and PAC-Fe electrodes.

As shown in Figure 9, the PAC-Fe composite exhibits a significantly higher energy density of 8.3 Wh kg^{-1} at a power density of 275.0 W kg^{-1} compared to the PAC electrode, which achieves 4.8 Wh kg^{-1} and 159.1 W kg^{-1}.

The enhanced energy and power densities in the PAC-Fe composite are attributed to the pseudocapacitive behavior of Fe_2O_3. The layered structure of Fe_2O_3 facilitates alkali ion intercalation/deintercalation during redox reactions, contributing to improved electrochemical performance.

3.2.5. Electrochemical impedance spectroscopy (EIS) analysis

Electrochemical impedance spectroscopy (EIS) was employed to analyze the resistive components of the PAC electrode and the PAC-Fe composite electrode (Figure 10). The

measurements were conducted in a 6 M KOH aqueous solution within a frequency range of 100 kHz to 0.1 Hz, using a perturbation signal with a 10 mV AC voltage.

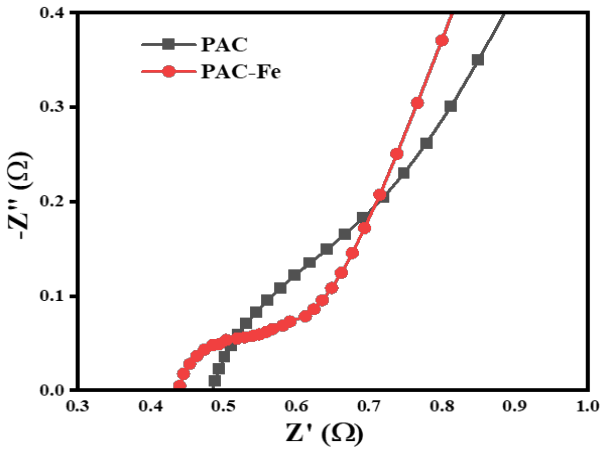

Fig. 10: Nyquist plot of PAC and PAC-Fe electrodes

As shown in Figure 10, the Nyquist plot exhibits a semi-circular loop in the high-frequency region and a linear line in the low-frequency region. The semi-circular loop represents the equivalent series resistance (ESR), which is the intercept of the semi-circle with the real axis (Z') at high frequency. The linear line in the low-frequency region is associated with ion diffusion within the electrode material (Shrestha, 2024).

By examining the intercept of the semi-circle with the real axis (Z') at high frequency, the ESR values can be estimated. The PAC electrode exhibits an ESR of approximately 4.9 Ω, while the PAC-Fe composite exhibits an ESR of approximately 4.4 Ω. The lower ESR value for the PAC-Fe composite indicates a lower internal resistance and better conductivity compared to the PAC electrode. The slope of the linear line in the low-frequency region is related to the Warburg impedance, which reflects the ion diffusion resistance. These results demonstrate that the incorporation of Fe_2O_3 into the PAC matrix significantly influences the resistive properties of the electrode.

2.4. Capacity Retention (%)

The cycling stability of the PAC and PAC-Fe electrodes was evaluated by measuring capacity retention after 1000 charge-discharge cycles at a current density of 3 A g^{-1} (Figure 11).

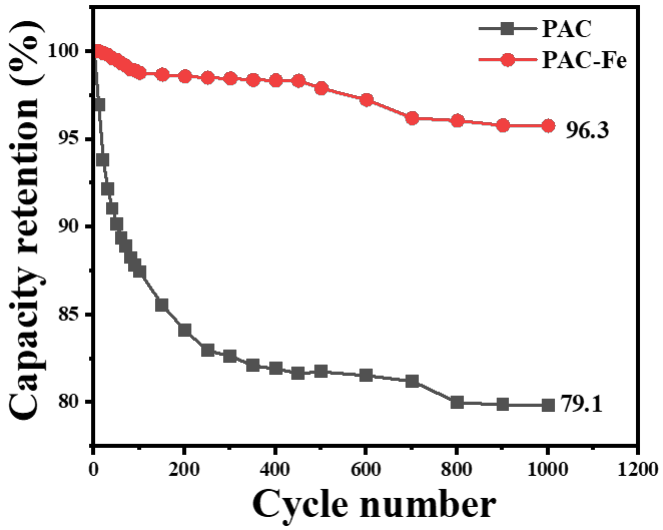

Fig.11: Capacity retention (%) of PAC and PAC-Fe electrodes after 1000 cycles at 3 A g^{-1}

As shown in Figure 11, the PAC electrode exhibited a capacity retention of 79.1% after 1000 cycles. In contrast, the PAC-Fe composite showed a significantly higher capacity retention of 96.3%, indicating improved stability compared to the pristine PAC electrode. The superior retention of the PAC-Fe composite suggests enhanced electrochemical stability, likely due to improved conductivity and reduced degradation. The incorporation of Fe_2O_3 into the PAC matrix appears to have a positive impact on the long-term stability of the electrode (Shrestha et al., 2019; Shrestha and Rajbhandari, 2021; Shrestha, 2022a; Shrestha, 2021).

4. Conclusion

This study synthesized and characterized activated carbon (PAC) derived from *Acacia catechu* waste wood for supercapacitor applications. The PAC material exhibited a high BET specific surface area of 989.4 m^2 g^{-1} and a surface rich in oxygenated functional groups. A facile method was developed to fabricate a hybrid nanocomposite electrode by combining PAC with Fe_2O_3 (PAC-Fe) at a 1:1 ratio. The electrochemical performance of both the PAC and PAC-Fe electrodes was evaluated, and the results are summarized in Table 1. The incorporation of Fe_2O_3 enhanced the electrochemical performance, as evidenced by the superior metrics of the PAC-Fe composite compared to the pristine PAC electrode. Specifically, the PAC-Fe electrode demonstrated:

- **Higher Specific Capacitance:** 104.3 F g^{-1} at 1 A g^{-1} (vs. 57.4 F g^{-1} for PAC)

- **Increased Energy Density:** 8.3 Wh kg^{-1} at a power density of 275.0 W kg^{-1} (vs. 4.7 Wh kg^{-1} at 159.1 W kg^{-1} for PAC)
- **Improved Capacitance Retention:** 96.3% after 1000 cycles at 3 A g^{-1} (vs. 79.1% for PAC)
- **Reduced ESR:** 0.43 Ω (vs. 0.49 Ω for PAC)
- **Wider Potential Window:** -1.15 V to -0.4 V (vs. -1 V to -0.2 V for PAC)

These enhancements are attributed to the synergistic effect between the high surface area of the activated carbon and the pseudocapacitive contribution of Fe_2O_3. The results suggest that the PAC-Fe nanocomposite holds promise as an electrode material for high-performance supercapacitors.

Table 1. Electrochemical Performance of PAC and PAC-Fe Electrodes

Electrodes	Potential window (v)	Specific capacitance(F g^{-1}) at 1 A g^{-1}	Energy density (W h kg^{-1})	Power density (W h kg^{-1})	Capacity Retension (%)	ESR(Ω)
PAC	-1 to -0.2	57.4	4.7	159.1	79.1	0.49
PAC:Fe	-1.15 to -0.4	104.3	8.3	275.0	96.3	0.43

Declarations

Author Contribution Statement

The author conducted all experiments, analyzed the data, and prepared the manuscript. The author also conceived and designed the research.

Data Availability Statement

The data associated with this study are available at Patan Multiple Campus, Tribhuvan University, Patandhoka, Lalitpur, Nepal.

Declaration of Interest Statement

The author declares no conflict of interest.

Acknowledgements

The author acknowledges Prof. Dr. Soo Wohn Lee of the Research Centre for Eco Multi-Functional Nano Material, Global Research Laboratory (GRL), Sun Moon University (SMU), South Korea, for providing laboratory facilities and guidance for advanced instrumental characterizations. The author also thanks Prof. Dr. Santi Maensiri of the School of Physics, Institute of Science, Suranaree University of Technology (SUT), Thailand, for providing access to electrochemical testing equipment and expertise.

References

Arun, T., Prabakaran, K., Udayabhaskar, R., Mangalaraja, R.V., Akbari- Fakhrabadi, A. (2019). Carbon decorated octahedral shaped Fe3O4 and a- Fe2O3 magnetic hybrid nanomaterials for next generation supercapacitor applications. Applied Surface Science. 485: 147–157.

Brunauer, S., Emmett, P., Teller, E. (1938). Adsorption of gases in multimolecular layers. Journal of American Chemical Society. 60:, 309–319

Chakraborty, S., Raj, M.A., Mary, N.L. (2020). Biocompatible Supercapacitor Electrodes Using Green Synthesised ZnO/Polymer Nanocomposites for Efficient Energy Storage Applications. Journal of Energy Storage. 28, 101275.

Gao, B., Li, Y., Tian, Y., Gai, L. (2017). Acidified Activated Carbon with Enhanced

Electrochemical Performance for Supercapacitors. International Journal of Electrochemical Science. 12, 116 – 127.

Kumari M, Radha, Kumar M, Zhang B, Amarowicz R, Puri S, Pundir A, Rathour S, Kumari N, Chandran D, Dey A, Sharma N, Rajalingam S, Mohankumar P, Sandhu S, Pant N, Ravichandran RP, Subramani M, Pandi K, Muthukumar M, Zengin G, Mekhemar M, Lorenzo J. M. (2022). Acacia catechu (L.f.) Willd. : A Review on Bioactive Compounds and Their Health Promoting Functionalities. Plants (Basel). 11(22), 3091.

Liu, Y., Wang, H., Zhou, J., Bian, L., Zhu, E., Hai, J. (2013). Graphene/polypyrrole intercalating nanocomposites as supercapacitors electrode, Electrochim. Acta, 112, 44–52.

Molina-Sabio, M., RodRiguez-Reinoso, F., Caturla, F., Sellés, M. J. (1995). Porosity in granular carbons activated with phosphoric acid, Carbon, 33, 1105-1113.

Sarangapani, S., Tilak, B.V., Chen, C. P. (1996). Materials for electrochemical capacitors theoretical and experimental constraints, J. Electrochem. Soc., 143, 3791-3799.

Sarkar, A., Singh, A. K., Sarkar, D., Khan, G.G., Mandal, K. (2015). Three-Dimensional Nano Architecture of BiFeO3 anchored TiO2 Nanotube Arrays for Electrochemical Energy Storage and Solar Energy Conversion, J. ACS Sust. Chem. Eng., 3(9), 2254-2263.

Shrestha, D. (2021). Efficiency of wood-dust of Dalbergia sisoo as low-cost adsorbent for

rhodamine-B dye removal. Nanomaterials, 11(9), 2217

Shrestha, D. (2022b). Evaluation of Physical and Electrochemical Performances of Hardwood and Softwood derived Activated Carbon for Supercapacitor Application. Mat. Sci. Ener. Techno, 5, 353-365.

Shrestha, D. (2022c). Activated carbon and its hybrid composites with manganese (IV) oxide as effectual electrode materials for high performance supercapacitor. Arabian J. Chem., 15(7), 103946.

Shrestha, D. (2022a). Nanocomposite electrode materials prepared from Pinus roxburghii and hematite for application in supercapacitors, Journal of the Korean Wood Science and Technology, 50(4), 219-236.

Shrestha, D. (2023). Applications of functionalized porous carbon from bio-waste of Alnus nepalensis in energy storage devices and industrial wastewater treatment. Heliyon, 9(11), e21804.

Shrestha, D. (2024). Structural and electrochemical evaluation of renewable carbons and their composites on different carbonization temperatures for supercapacitor applications. Heliyon, 10(4, e25628).

Shrestha, D., Gyawali, G., Rajbhandari, A. (2018). Preparation and Characterization of Activated Carbon from Waste Sawdust from Saw Mill. J. Sci. Techno, 22(2), 103- 108.

Shrestha, D., Maensiri, S., Wongpratat, U., Lee, S.W., Rajbhandari, A. (2019). Shorea robusta derived activated carbon decorated with manganese dioxide hybrid composite for improved capacitive behaviors. Journal of Environment and Chemical Engineering, Elsevier 7, 103227.

Shrestha, D., Rajbhandari, A. (2021). The effects of different activating agents on the physical and electrochemical properties of activated carbon electrodes fabricated from wood-dust of Shorea robusta. Heliyon. 7: e07197.

Sinprachim, T., Phuming, S., Maensiri, S. (2016). Electrochemical energy storage performance of electrospum AgOx-MnO2/CNF composites, J. Alloys Compd., 677, 1–11.

Wang, C., Li, H., Zhao, J., Zhu, Y. (2013). Graphene nanoribbons as a novel support material for high performance fuel cell electro catalysts, Int. J. Hydro. Ener, 38, 13230–13237.